(TITLE UNCLASSIFIED)

INVESTIGATION OF STATIC STABILITY AND AERODYNAMIC EFFECTS OF CONTROL JETS ON A 1/3-SCALE PYE WACKET MISSILE AT SUPERSONIC SPEEDS

By

A. Anderson
VKF, ARO, Inc.

March 1961

This document has been approved for public release and sale; its distribution is unlimited.

AFletter, 25 Aug 70, Signed William O. Cake
9-1-70

ARNOLD ENGINEERING DEVELOPMENT CENTER

AIR RESEARCH AND DEVELOPMENT COMMAND

AF

(Title Unclassified)

INVESTIGATION OF STATIC STABILITY AND AERODYNAMIC EFFECTS OF CONTROL JETS ON A 1/3-SCALE PYE WACKET MISSILE AT SUPERSONIC SPEEDS

By

A. Anderson
VKF, ARO, Inc.

March 1961

ARDC Program Area 740A, Project No. 3811
ARO Project No. 331058

Contract No. AF 40(600)-800 S/A 11(60-110)

ABSTRACT

Tests were conducted on a 1/3-scale model of the Pye Wacket missile in the 40-inch supersonic wind tunnel of the von Kármán Gas Dynamics Facility at Mach numbers from 1.5 to 5 and Reynolds numbers per inch from 0.08 to 0.47 million.

Static stability characteristics and detailed pressure distributions were obtained at simulated forward, side, and aft launch conditions, at angles of attack from -5 to 15 deg, and at yaw angles from 0 to 180 deg. The influence of control jets on the surface pressure distributions and the interaction forces produced by the jets are shown.

CONTENTS

	Page
ABSTRACT	2
NOMENCLATURE	5
INTRODUCTION	7
APPARATUS	
Wind Tunnel	7
Models	7
Instrumentation and Precision of Measurements	8
PROCEDURE AND TEST CONDITIONS	9
RESULTS AND DISCUSSION	11
CONCLUSIONS	13
REFERENCES	13

TABLES

1.	Force Model Test Summary	14
2.	Pressure Model Test Summary	15

ILLUSTRATIONS

Figure		
1.	Tunnel A, a 40 by 40-in. Supersonic Wind Tunnel	16
2.	Sketches of Models	17
3.	Model Photographs	19
4.	Longitudinal Stability Characteristics at $M_\infty = 3$	20
5.	Variation of Aerodynamic Parameters with Mach Number	21
6.	Variation of Axial-Force Coefficient with Angles of Attack and Yaw	22
7.	Variation of Lateral Stability Characteristics with Yaw Angle	23
8.	Typical Schlieren Photographs of Force Model	24
9.	Longitudinal Stability Characteristics with Jet Flow Effects at $M_\infty = 2$	25

Figure		Page
10.	Effect of Windward Surface Jet Flow on Pitching-Moment and Normal-Force Coefficients	26
11.	Effect of Jet Pressure Ratio on Normal-Force and Pitching-Moment Coefficients at $M_\infty = 2$	27
12.	Pressure Isolines p/p_∞ on the Windward Surface at $M_\infty = 2$, $\alpha = 6$ deg	28
13.	Photographs of Flow Patterns on Wind Surface at $M_\infty = 2$, $\alpha = 6$ deg	29
14.	Typical Schlieren Photographs of Pressure Model	30

NOMENCLATURE

A_b	Base area, 60.1 sq in.
C_A	Total axial-force coefficient, total axial force/$q_\infty S$
C_{A_b}	Base axial-force coefficient, $(p_\infty - p_b)A_b/q_\infty S$
C_ℓ	Rolling-moment coefficient, rolling moment/$q_\infty Sd$
C_m	Pitching-moment coefficient, pitching moment/$q_\infty Sd$ (see Fig. 2 for moment reference point)
C_{m_α}	Slope of the pitching-moment coefficient curve, $dC_m/d\alpha$ at $\alpha = 0$, per deg
C_{m_j}	Equivalent pitching-moment coefficient caused by the jet thrust, jet pitching moment/$q_\infty Sd$
C_N	Normal-force coefficient, normal force/$q_\infty S$
C_{N_j}	Equivalent normal-force coefficient caused by the jet thrust, jet thrust/$q_\infty Sd$
C_{N_α}	Slope of the normal-force coefficient curve, $dC_N/d\alpha$ at $\alpha = 0$, per deg
C_n	Yawing-moment coefficient, yawing moment/$q_\infty Sd$ (see Fig. 2 for moment reference point)
C_Y	Side-force coefficient, side force/$q_\infty S$
ΔC_m	Change in pitching-moment coefficient $(C_{m_{jets\ on}} - C_{m_{jets\ off}})$ obtained from integration of the model surface pressures
ΔC_N	Change in normal-force coefficient $(C_{N_{jets\ on}} - C_{N_{jets\ off}})$ obtained from integration of the model surface pressures
d	Model diameter, 20 in.
M_∞	Free-stream Mach number
p	Model pressure, psia
p_b	Base pressure, psia
p_e	Jet exit static pressure, psia
p_o	Stilling chamber pressure, psia
p_{o_j}	Jet stagnation pressure, psia
p_∞	Free-stream static pressure, psia

q_∞	Free-stream dynamic pressure, psia
Re	Reynolds number
S	Model planform area, 314.16 sq in.
T_o	Stilling chamber temperature, °R
X_{cp}	Distance from center of pressure to model centerline in body diameters, C_{m_s}/C_N (positive forward)
α	Angle of attack, deg
ψ	Angle of yaw, deg
ϕ	Angle of roll, deg

SUBSCRIPTS

s	Stability axis

MISSILE STABILITY AXIS SYSTEM

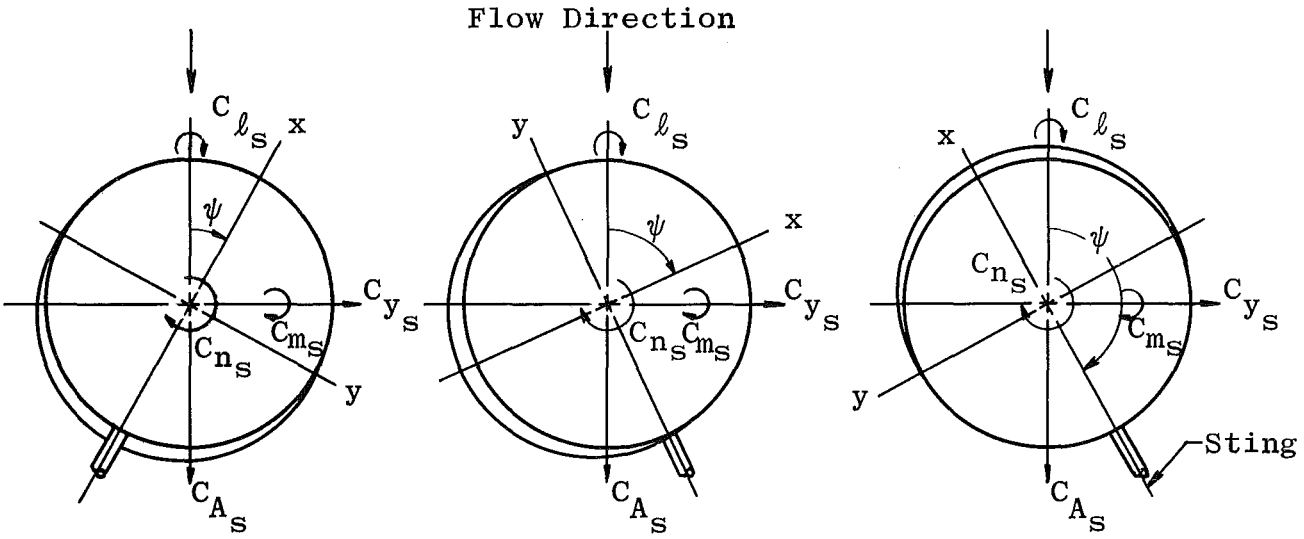

Positive Direction Shown by Arrows

Forward Launch Side Launch Aft Launch

Note: Stability axis system is in the plane of the missile and fixed with respect to the free-stream flow direction.

INTRODUCTION

Tests were conducted in the 40 by 40-in. supersonic wind tunnel of the von Kármán Gas Dynamics Facility (VKF), Arnold Center, during the period October 12 to October 26, 1960, for the Pomona Division of Convair at the request of the Air Proving Ground Center (APGC), Eglin Air Force Base.

The tests were made to provide aerodynamic data necessary for development of a Feasibility Test Vehicle (FTV) of the Pye Wacket, a lenticular-shaped air-to-air missile. A previous investigation in Tunnel A of lenticular configurations for the Pye Wacket by Convair is reported in Ref. 1.

The test objective was to measure the static stability and drag characteristics of a 1/3-scale Pye Wacket FTV missile at simulated forward, side, and aft launch conditions encountered in omnidirectional launches and to obtain detailed surface pressure distributions over the model to investigate the influence of reaction jets on the missile aerodynamic characteristics. The force and pressure distribution tests were conducted at Mach numbers from 1.5 to 5.

APPARATUS

WIND TUNNEL

Tunnel A (Fig. 1) is a 40 by 40-in., continuous, closed circuit, variable-density, supersonic wind tunnel with a Mach number range from 1.5 to 6. The top and bottom walls of the nozzle are flexible plates which are automatically positioned at the desired contours by electrically driven screw jacks. The tunnel is driven by a 100,000 horse-power compressor system which provides maximum tunnel stagnation pressures of 2 to 13.5 atmospheres at $M_\infty = 1.5$ and $M_\infty = 6$, respectively. Minimum operating pressures are less than one tenth of the maximum. A complete description of the tunnel may be found in Ref. 2.

MODELS

Two 1/3-scale models were furnished by Convair, a force model and a pressure model, each having circular planforms 20 inches in diameter.

Manuscript released by author February 1961.

The models were fabricated from aluminum and were capable of being sting mounted at three positions 90-deg apart to simulate a forward, side, and aft launch condition (Fig. 2). The hemispherical nose piece (Fig. 2a) was tested on the force model only.

The pressure model (Fig. 2b) was instrumented with 86 orifices on one surface, 5 orifices on the leading edge, and 6 orifices on the model base. The two reaction jets on this model (see Fig. 2b) had 0.25-in.-diam throats and expansion ratios of three and were positioned so that the jet-nozzle exits were flush with the model surface.

Installation photographs of the models are given in Fig. 3. The photograph of the pressure model installation shows the disposition of pressure tubing along the sting-support and the flexible lines used to supply high-pressure air to the jet nozzles.

INSTRUMENTATION AND PRECISION OF MEASUREMENTS

Model surface pressures aft of the leading edge were measured on an eight-unit, eleven-port-valve system, each valve of which was connected to two differential transducers of 1 and 15-psi capacity which had essentially a vacuum for a reference pressure. The sensitivity of each transducer was adjusted to give full-scale readings at pressures of approximately one-fourth, one-half, and maximum capacity. Thus a total of six pressure ranges could be selected (dependent upon the level of the pressure to be measured) ranging from 15 to 0.25 psia. The uncertainty of these transducers is considered to be not more than ±0.035 and ±0.002 psi at the 15 and 0.25 psi pressure levels, respectively.

Pressures at the model leading edge and base were also measured on differential pressure transducers referenced to a near vacuum, and any one of three transducers of 1, 5, and 15-psi capacity could be selected for each pressure measurement. These transducers have an uncertainty of not more than 0.5 percent of their rated capacity.

The reaction-jet stagnation pressures were measured on 1500-psi absolute pressure transducers which were located in the chamber of each jet. The transducers were supplied by Convair and calibrated at VKF. From the calibration data it is estimated that these measurements have an uncertainty of about ±5 psia.

Force and moments were measured with an internal, six-component, strain-gage balance furnished by Convair and calibrated at VKF. A

standard statistical analysis of the balance calibration data indicates the uncertainties of the forces and moments to be as given below:

	Design Load	Uncertainty	Coefficient
Normal Force	±1000 lb	±8.4 lb	±.007
Pitching Moment	±3000 in.-lb	±8.1 in.-lb	±.0003
Side Force	±400 lb	±3.2 lb	±.003
Yawing Moment	±1000 in.-lb	±21.8 in.-lb	±.0009
Rolling Moment	±1120 in.-lb	±5.0 in.-lb	±.0002
Axial Force	200 lb	±0.8 lb	±.0006

The coefficient uncertainties given above were obtained by using the value of free-stream dynamic pressure, q_∞ = 4 psia, at which most of the data were taken.

The force and pressure data and other measurements, such as angle of attack, jet chamber pressure and temperature, and tunnel stagnation pressure and temperature were processed with the VKF automatic data handling system and ERA 1102 computer. The model surface pressure distributions were integrated to obtain aerodynamic coefficients by a numerical integration process on an IBM 7070 computer.

PROCEDURE AND TEST CONDITIONS

Force and pressure data were obtained with the model supported at three sting positions which provided an angle-of-yaw coverage of 0 to 15 deg, 75 to 105 deg, and 165 to 180 deg. Remote roll operation of the model also allowed an angle-of-attack range from -5 to 15 deg and combined angles of attack and yaw during a given run. These conditions and the test Mach numbers for each model configuration are listed in Tables 1 and 2 for the force and pressure test phases, respectively. Table 2 also shows the stagnation pressure values of the reaction jets during the pressure phase tests. Measurements of the jet chamber temperatures showed these to be relatively constant with jet pressure level and equal to about 50°F ±10°F.

No base pressure measurements were taken during the force tests; however, a base axial force was computed during the pressure phase tests by using an arithmetic average of the six pressure measurements at the model base.

With the force model in the aft-launch position, data were taken at a reduced pressure level (q_∞ = 2 psia) because of the large axial forces

encountered and the limit balance axial-force loading of 200 lb. Also, tests at Mach number 2 were discontinued because of large fluctuations of the model wake caused by reflected shock interaction close to the model base. Similar interference was observed at Mach number 1.5 with the model in the side-launch position.

Force and moment data were computed in the body axes and an axis which remains fixed with respect to the free-stream flow direction. This axis system will be referred to as the stability axis in this report. For all coefficients the model planform area and diameter were used for the reference area and length, respectively. Moment coefficients were computed about the body mid-chord point (see Fig. 2), and the angles of attack and yaw were corrected for deflection of the sting support caused by airloads on the model.

The tunnel conditions for the pressure and force test phases are listed in the following table:

Nominal M_∞	Calibrated M_∞	p_o, psia	T_o, °R	Re/in. x 10^{-6}	Remarks
1.5	1.50 ±.01	9	554	0.22*	
2	1.99 ±.01	11.5	555	0.22	
		8		0.18	Pressure Test Only
		5		0.10	Pressure Test Only
2.5	2.49 ±.01	8	555	0.13**	Force Test Only
3	3.00 ±.01	32	560	0.39	Force Test Only
		24		0.29*	
		12		0.15**	
		6		0.08	Force Test Only
4	4.02 ±.01	55	564	0.40*	
5	5.09 ±.02	125	630	0.47*	

* Test Reynolds number corresponding to q_∞ = 4 psia
** Test Reynolds number for aft launch condition in force tests

RESULTS AND DISCUSSION

Data are presented from the force model tests in Figs. 4 through 7 and are given in terms of the missile stability axis system as defined in the Nomenclature. In Fig. 4 the longitudinal stability characteristics of the model at each of the three launch conditions are given for Mach number 3. These results show that the body is unstable about the mid-chord point for each launch condition; the side-launch case has the most forward center-of-pressure location, while the center-of-pressure locations for the forward and aft launch cases are about the same. (It should be noted here that the pitching moment in the stability axis system is always positive for leading edge up relative to the flow direction.)

The trends shown in Fig. 4 for data at Mach 3 were similar at other Mach numbers as shown in the parameter plots given in Fig. 5. Data obtained with the hemisphere-cylinder nose on the model (see Fig. 2a) show that the nose had only a small effect upon these parameters. On the plot given for the variation of the axial-force coefficient with Mach number at zero angle of attack, the base axial-force coefficients have been included as computed from the pressure test results for the model in forward launch. Reynolds number effects on the stability parameters in Fig. 4 were very small for the Reynolds numbers tested and were therefore not presented.

The variation of the axial-force coefficient with angles of attack and yaw are given in Fig. 6. These data, as plotted, show only small variations with yaw angle with respect to the launch attitude; however, the variation is large when the data are viewed in terms of model yaw angles of from -5 to 15 deg for the model in forward launch (Fig. 6b), 76 to 104 deg for the side-launch data (Fig. 6c), and 166 to 180 deg for the aft-launch case (Fig. 6b).

Coefficients of side force, yawing moment, and rolling moment for Mach numbers 2 and 3 have been plotted against the model yaw angles (as noted above) in Fig. 7 to show the variation in these coefficients as the model is yawed from 0 to 180 deg. The side-force coefficient variation with yaw angle shows that the maximum side force will occur between ψ = 90 and 180 deg because of the pressure forces on the blunt windward face (model base). Also within the region ψ = 90 to 180 deg the yawing-moment coefficient changes from negative to positive, and the missile becomes statically unstable in yaw.

The data also show that an increase in angle of attack had the most notable effect upon the yawing-moment coefficients for the side launch

attitude particularly at yaw angles close to 90 deg. This effect was more pronounced at the lower Mach number, $M_\infty = 2$. A considerable change in rolling moment was obtained with an increase in angle of attack as is shown in Fig. 7c. At zero angle of attack the rolling-moment coefficients were or near zero for the yaw angles tested. Schlieren photographs of the force model in each launch position are given in Fig. 8.

Typical results from the pressure model tests, showing the influence of the reaction jets upon the model normal-force and pitching-moment coefficients, the effects of the jet force caused by aerodynamic interaction, and surface pressure distributions are presented in Figs. 9 through 12. The coefficients of normal force and pitching moment presented here were obtained from a numerical integration of the measured surface pressures and therefore do not include the jet reaction forces. Also, since the model was instrumented with orifices and jets on one side only, it is assumed that the jet flow did not influence the surface pressures on the opposite side from the jets.

The interaction of the jets with the airflow over the model surface in effect creates a local high-pressure region in much the same manner as a deflected aerodynamic control surface and increases the normal force and pitching moment. The data given in Fig. 9 for the variation of normal-force and pitching-moment coefficient with jets on for the model in the forward launch position at $M_\infty = 2$ show this pronounced effect. The windward surface jets produced a positive normal-force increment and a negative (stabilizing) pitching-moment increment. Similarly, a negative normal-force increment and a positive pitching-moment increment are obtained with the jets on the leeward surface. Also shown in this figure are data obtained from the force model tests on this configuration; these data agree quite well with the jets-off data from the pressure tests. It should be pointed out here, however, that the pressure results do not include any correction to the angles of attack for sting deflections under air loads.

The normal-force and pitching-moment increments (jets on - jets off) produced by the windward surface jets at the forward launch attitude over the Mach number range are shown for various angles of attack in Fig. 10. These results show a trend of increasing interaction effect as angle of attack increases at each Mach number. Included for comparison in this figure are the calculated coefficients, C_{N_j} and C_{m_j}, caused by the jet reaction force. This comparison shows that the augmentation of the jet reaction forces by the interaction effect is of considerable magnitude. The effect of varying the jet pressure ratio on the normal-force and pitching-moment coefficient is shown in Fig. 11 for the windward

jets on in forward launch attitude at $M_\infty = 2$. These data show that the effect of angle of attack decreases as the jet pressure ratio decreases at a given Mach number and free-stream pressure.

In Fig. 12 pressure isoline charts of the windward surface with jets on and jets off at $M_\infty = 2$ and $\alpha = 6$ deg are shown for the model in the forward launch attitude. A comparison of the charts shows that the effect of the jets extends up to the leading edge of the model. This extension would indicate a general thickening of the boundary layer up to the leading edge caused by the strong shock system produced by the jet airstream interaction. Flow patterns on the model surface at the same test condition were obtained by an oil-film technique. Photographs of these patterns (Fig. 13) show very clearly the extent of the primary interference of the reaction jets upon the model surface flow. Typical schlieren photographs of the pressure model with jets on are given in Fig. 14.

CONCLUSIONS

1. The model was longitudinally unstable at all three launch positions.
2. At yaw angles between 90 and 180 deg the model becomes laterally unstable.
3. The control effectiveness of the reaction jets was increased quite markedly as a result of aerodynamic interactions.
4. The control force augmentation produced by the jet interaction increased as angle of attack increased; however, this effect decreased as the jet pressure ratio decreased at a given Mach number and free-stream conditions.

REFERENCES

1. Anderson, A. "Force Tests of Lenticular Configurations at Supersonic Speeds." AEDC-TN-60-51, March 1960. (Secret)
2. Schueler, C. J. and Strike, W. T. "Calibration of a 40-Inch Continuous Flow Tunnel at Mach Numbers 1.5 to 6." AEDC-TN-59-136, November 1959.

TABLE 1

FORCE MODEL TEST SUMMARY

Model Attitude and Configuration	Nominal Mach Number						Roll Angle ϕ, deg	α
	1.5	2	2.5	3	4	5		
Forward Launch	x	x		x	x	x	0, 90	A
Forward Launch				x	x	x	*Varied	B
Forward Launch		x					*Varied	C
Forward Launch	x						*Varied	D
Forward Launch with Nose	x			x			0, 90	A
Forward Launch with Nose				x			Varied	B
Forward Launch with Nose	x						Varied	C
Side Launch		x		x			0, 90, -90	A
Side Launch				x			Varied	B
Side Launch		x					Varied	C
Side Launch with Nose		x					0, 90, -90	A
Side Launch with Nose		x					Varied	D
Aft Launch			x	x			0, 90	A
Aft Launch			x	x			Varied	B

*Model rolled and pitched to obtain data in yaw for each of the indicated angles of attack

A = -5 to 15 deg
B = 3, 6, 9, and 12 deg
C = 3, 6, and 9 deg
D = 3 and 6 deg

TABLE 2

PRESSURE MODEL TEST SUMMARY

Model Attitude	Nominal Mach No.	Jet Pressure, psia		Angle of Attack α, deg
		$p_{o_{jL}}$	$p_{o_{jR}}$	
Forward Launch	1.5	0	0	0, 6, 12
		550	550	0*, 6*, 12*
		700	0	0, 6
		700	700	0, 6, 12
	2	0	0	0, 3, 6, 9, 12, 14, A, B
		400	400	0, 3, 6*, 9*, 12
		500	500	0
		550	550	6
		50-700	0	3, 6, 9, 12, A
		0	700	0, A
		700	700	0, 3, 6, 9, 12, A
		850	850	0, 6
	3	0	0	0, 3, 6, 9, 12, 14, C
		400	400	0, 6*
		700	0	0, 3, 6, 12
		700	700	0, 3*, 6, 9, 12*, 14*
	4	0	0	0, 3, 6, 12
		700	0	3, 6, 12
		700	700	3, 6, 12
	5	0	0	0, 3, 12
		700	700	0, 3
Side Launch	2	0	0	0, 3, 6, 9, 12, ±A
		550	550	±A
		700	0	0, 3, 6, 9, 12, ±A
		0	700	0, 3, 6, 9, 12, ±A
		700	700	0, 3, 6, 9, 12, ±A
	3	0	0	0, 3, 6
		0	700	0
		700	0	0
		700	700	0
Aft Launch	3	0	0	0, 3, 6, 14*, A
		700	700	0, 3, 6, A

Legend

* Windward surface only
A. Also at ψ = 14 deg
B. Also ψ = 3, 6, 9, and 12 deg with constant α = 6 deg
C. Also ψ = 3, 6, 9, deg with constant α = 6 deg

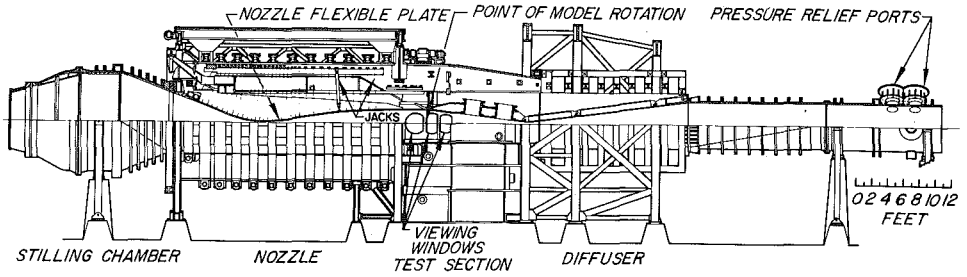

Assembly

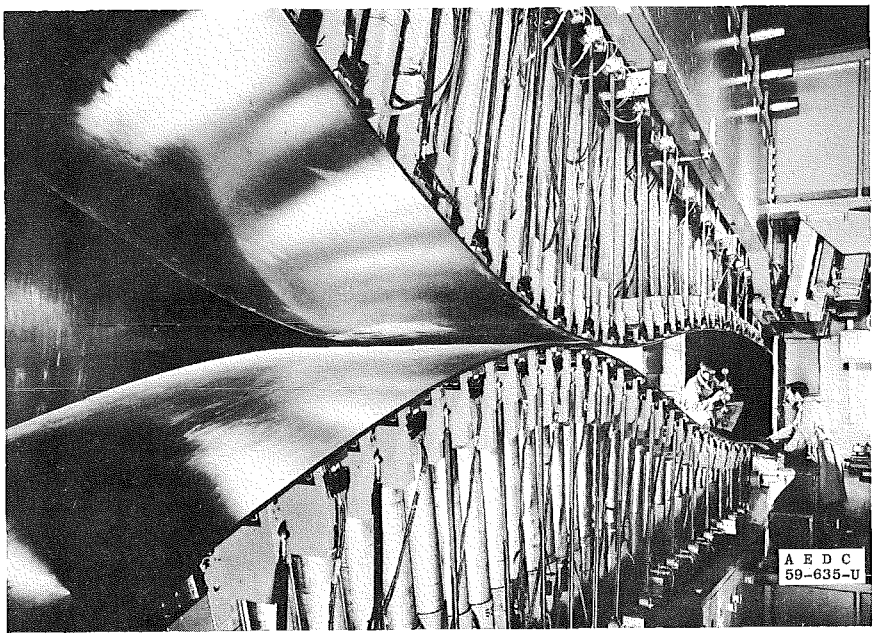

Fig. 1 Tunnel A, a 40 by 40-in. Supersonic Wind Tunnel

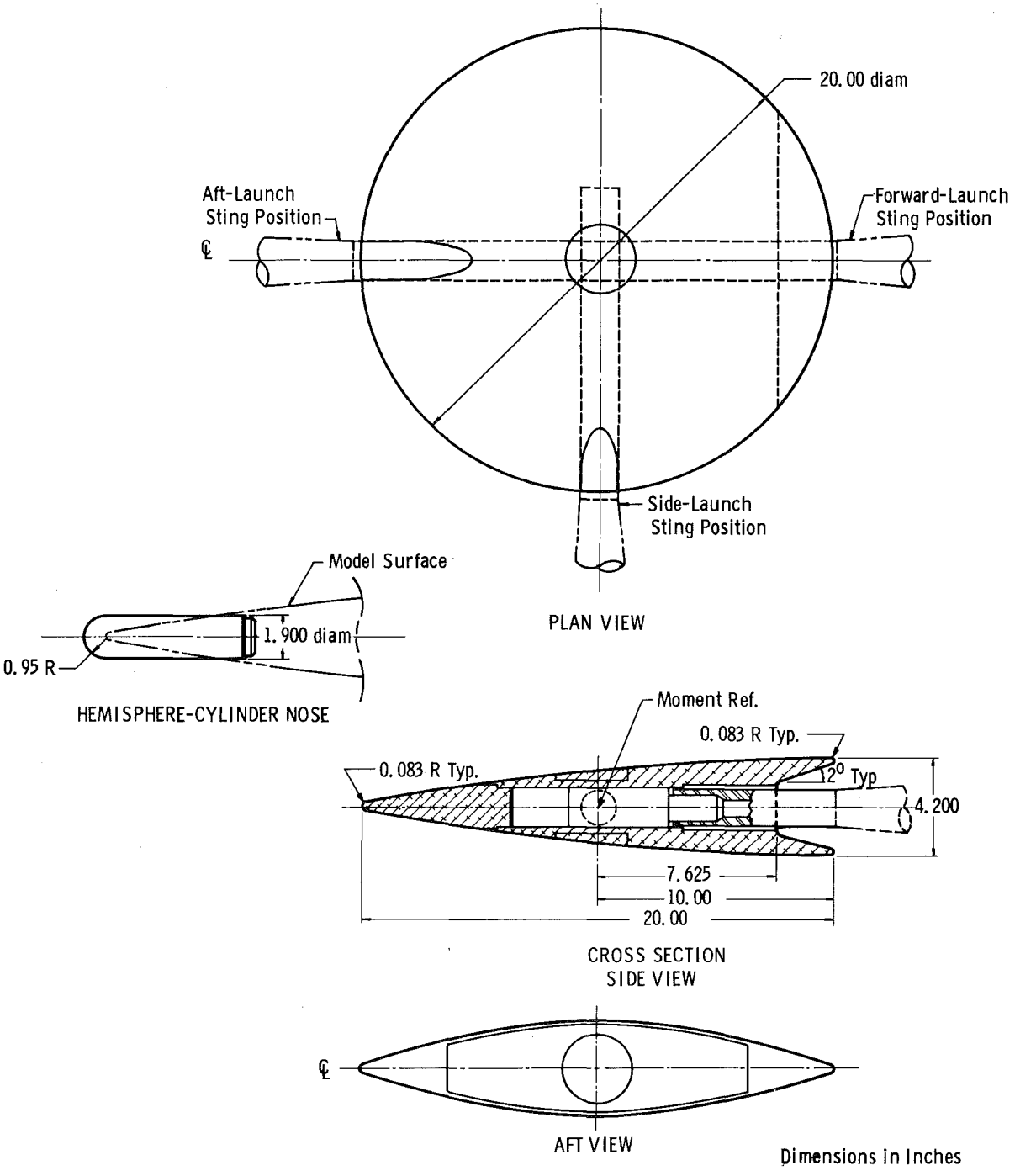

a. Force Model

Fig. 2 Sketches of Models

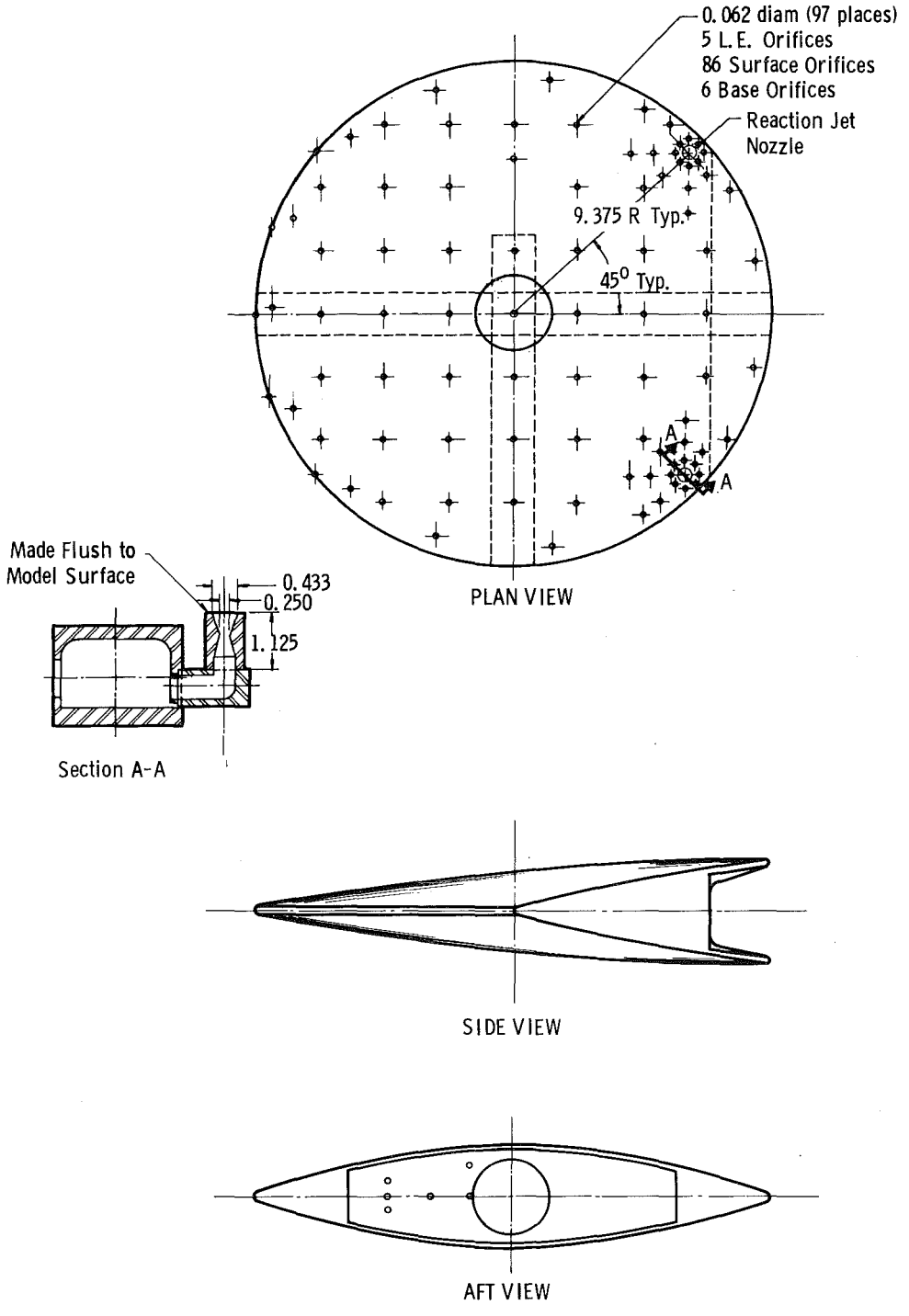

b. Pressure Model

Fig. 2 Concluded

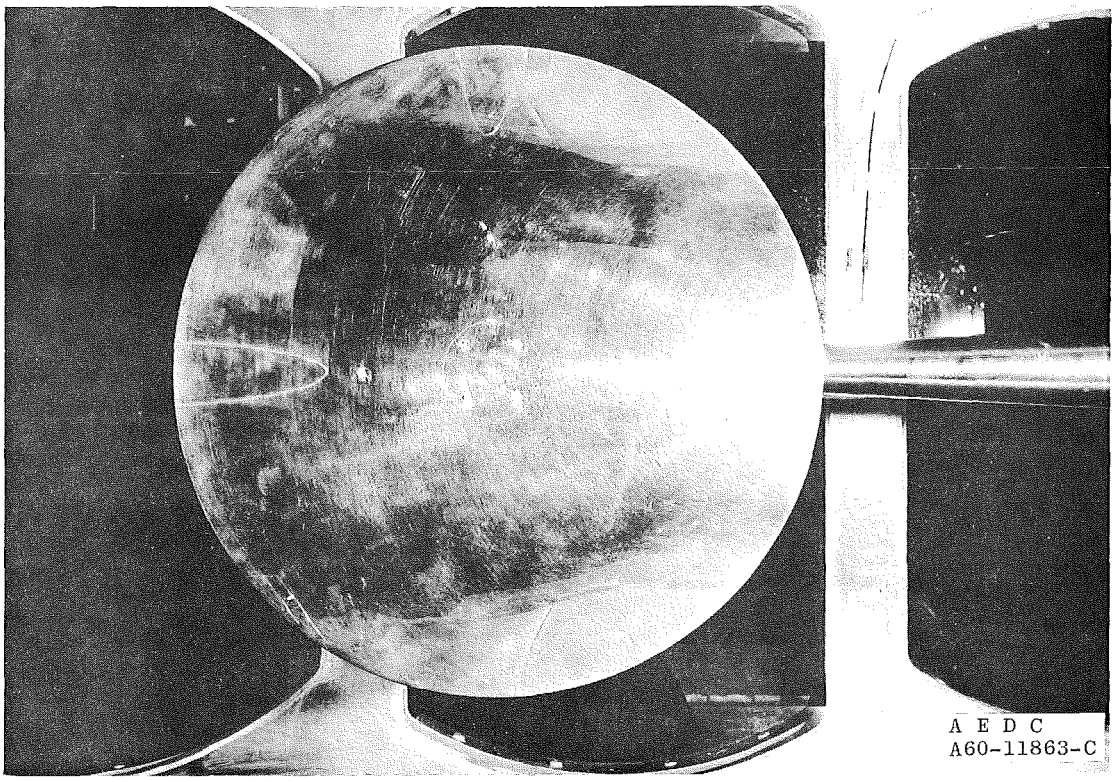

a. Force Model in Forward Launch Position

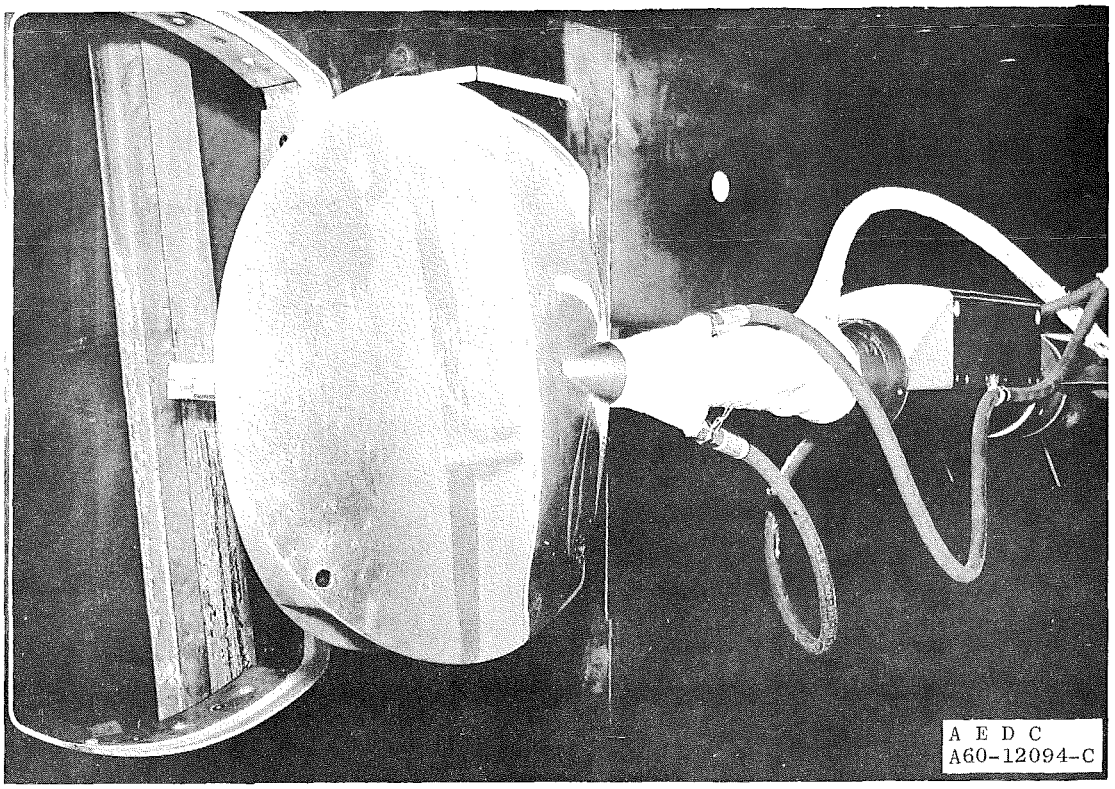

b. Pressure Model in Side Launch Position

Fig. 3 Model Photographs

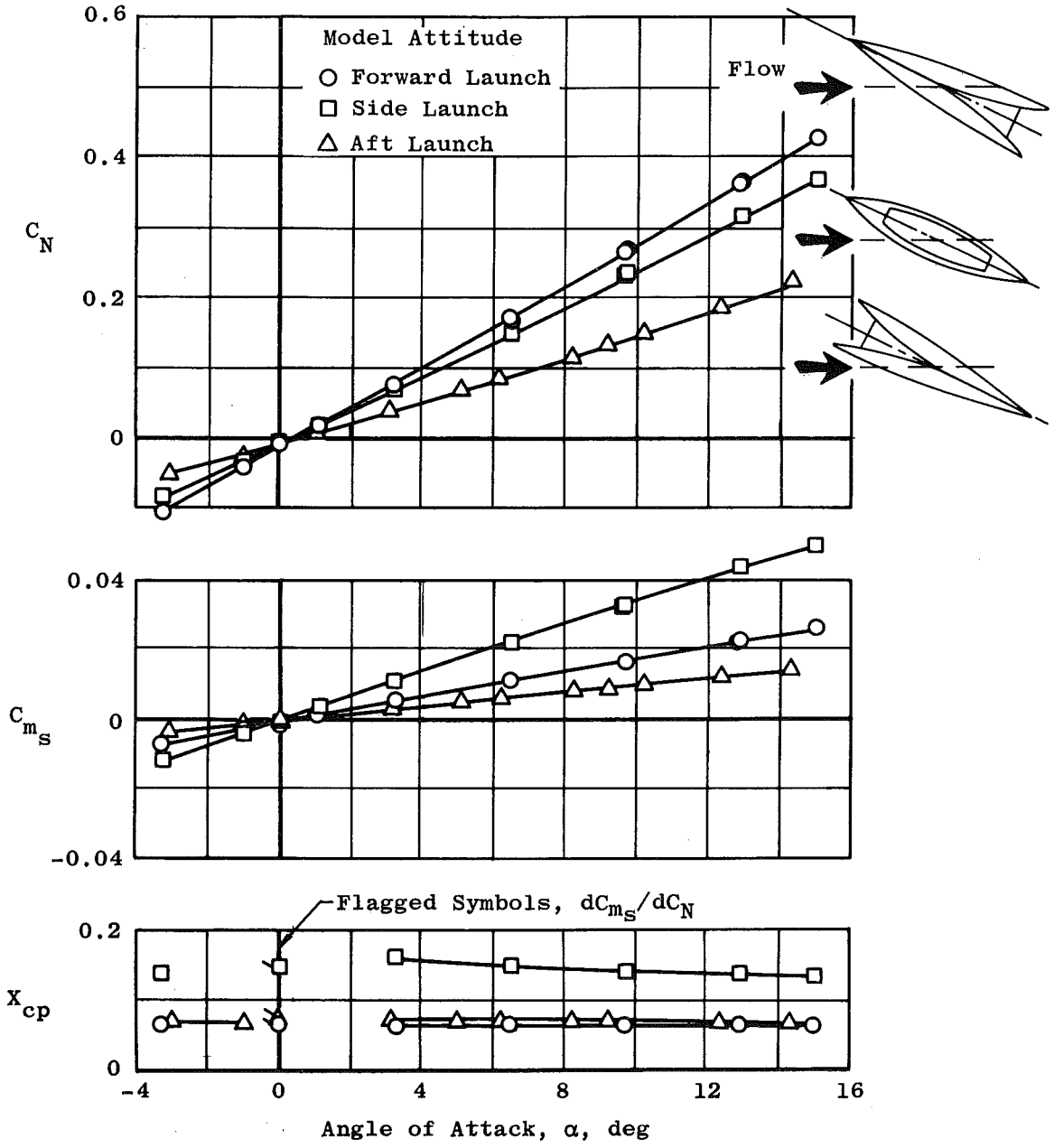

Fig. 4 Longitudinal Stability Characteristics at $M_\infty = 3$

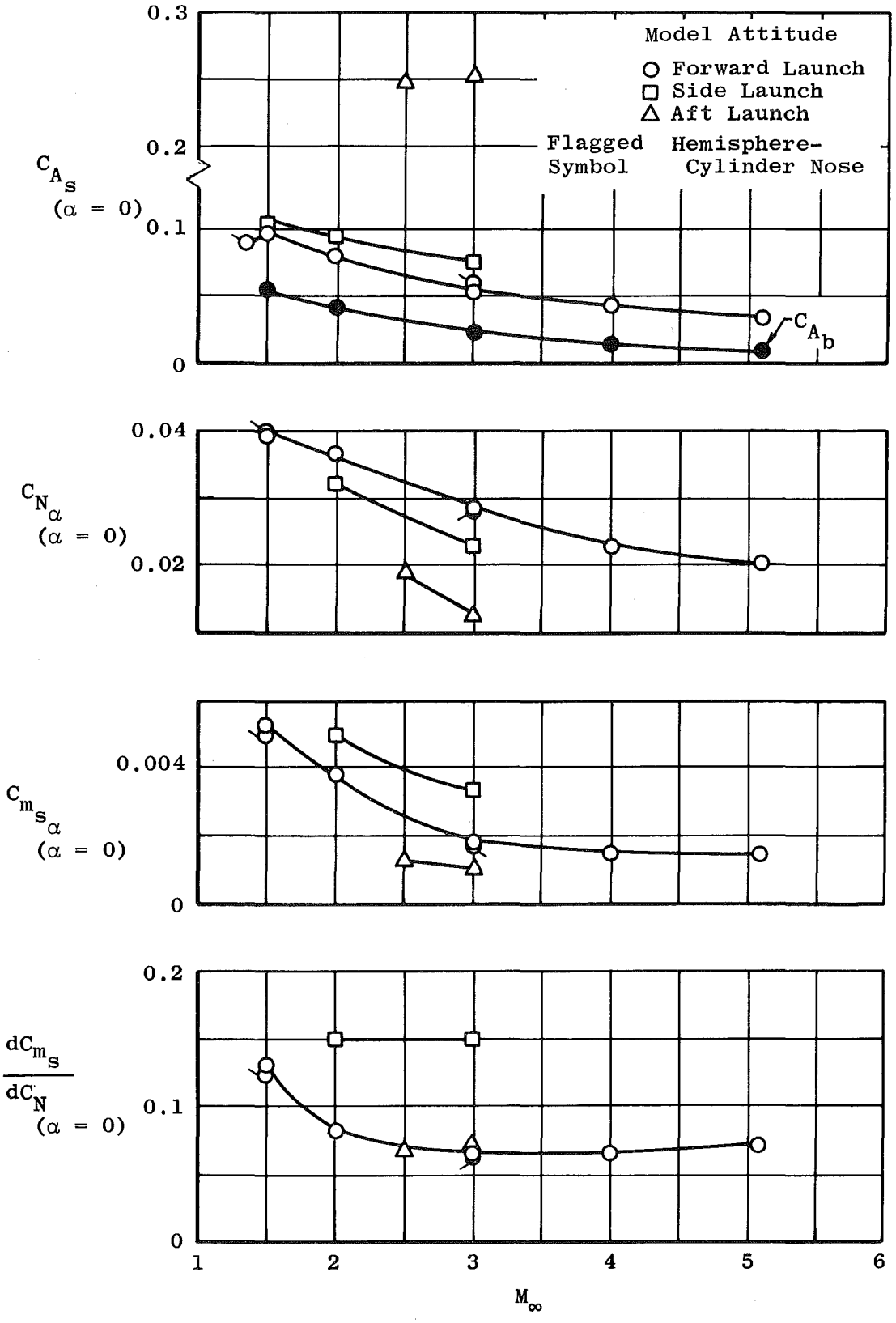

Fig. 5 Variation of Aerodynamic Parameters with Mach Number

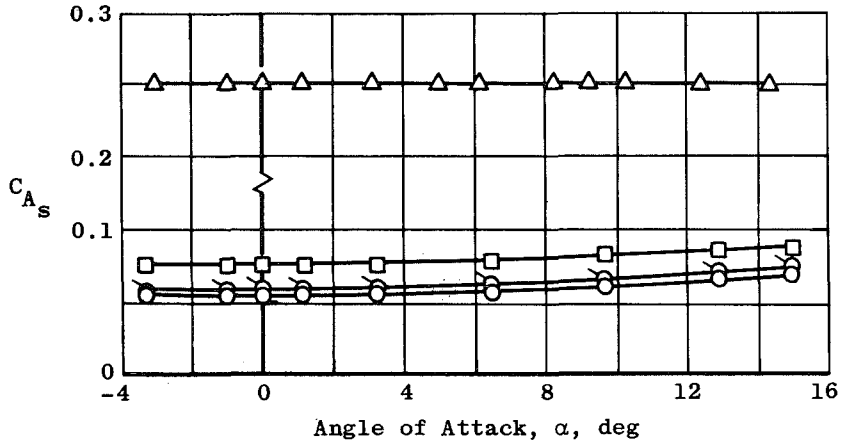

a. Variation of C_{A_s} with α at $M_\infty = 3$

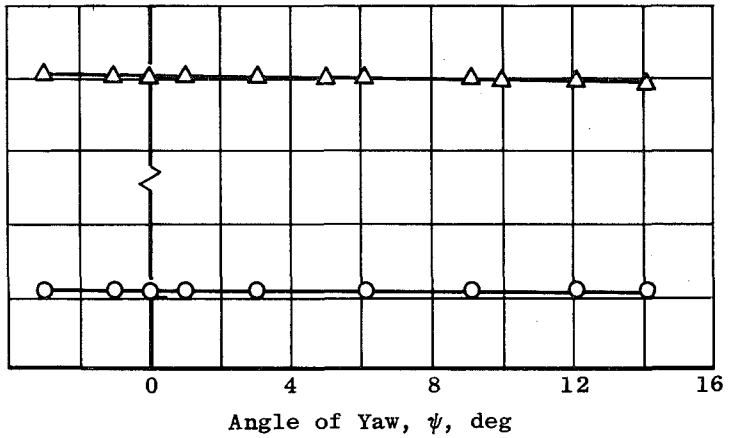

b. Variation of C_{A_s} with ψ at $M_\infty = 3$

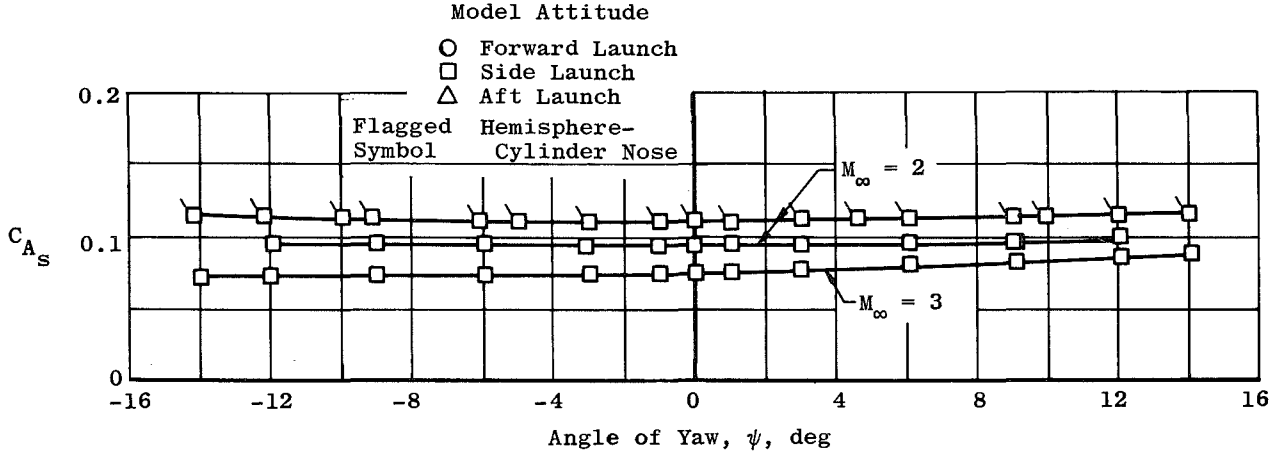

c. Variation of C_{A_s} with ψ at $M_\infty = 2$ and 3, Side Launch Attitude

Fig. 6 Variation of Axial-Force Coefficient with Angles of Attack and Yaw

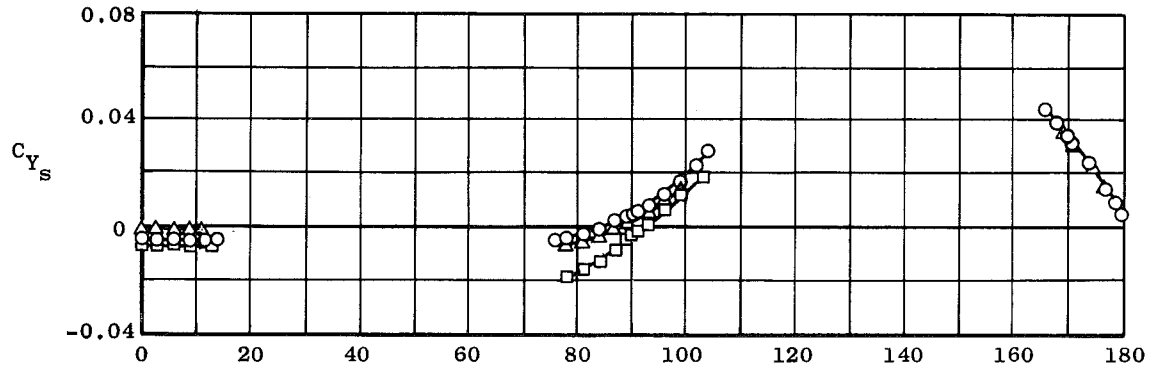

a. Side-Force Coefficient

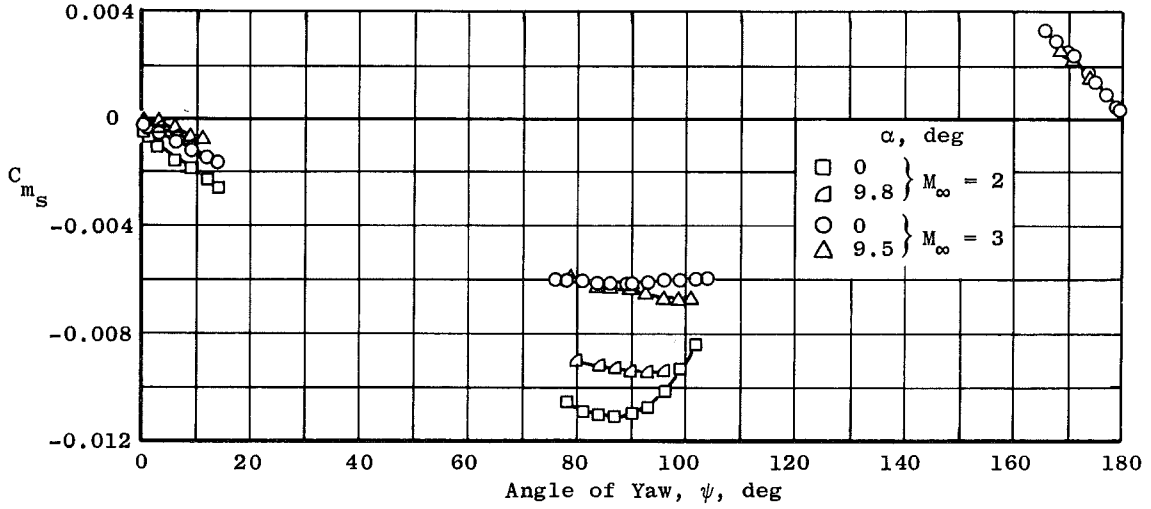

b. Yawing-Moment Coefficient

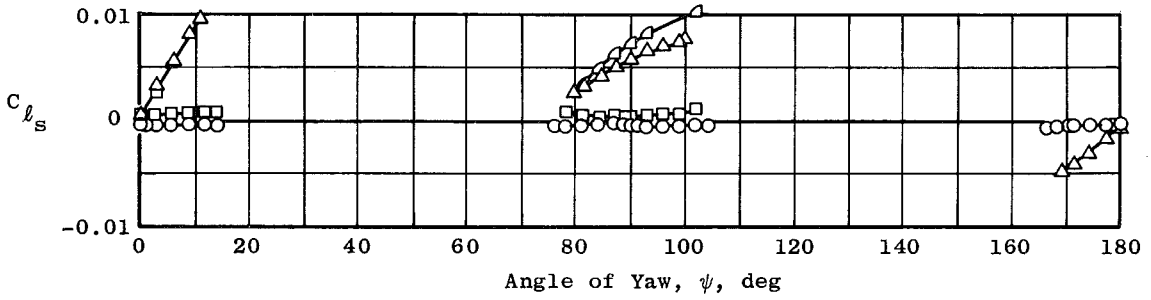

c. Rolling-Moment Coefficient

Fig. 7 Variation of Lateral Stability Characteristics with Yaw Angle

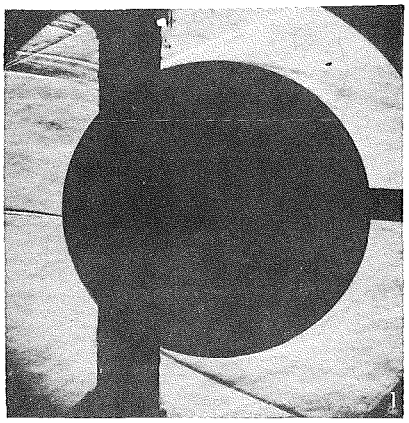

$M_\infty = 3$

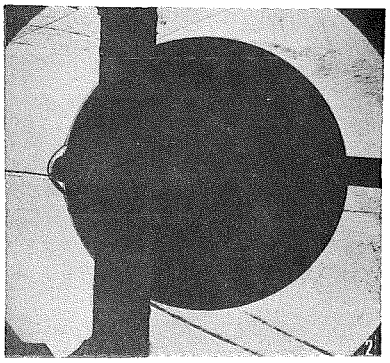

$M_\infty = 3$ (Nose Configuration)

Forward Launch Attitude

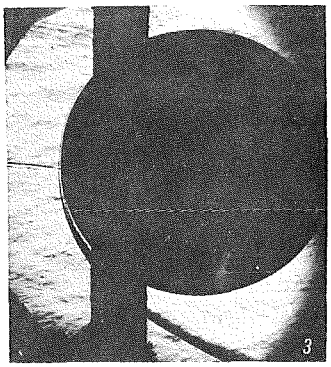

$M_\infty = 3$

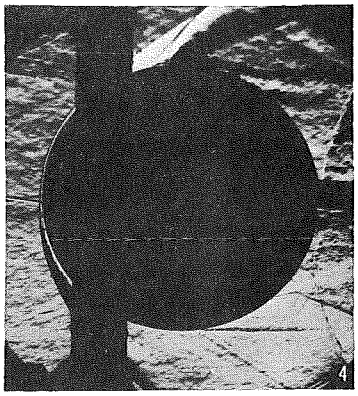

$M_\infty = 2$ (Nose Configuration)

Side Launch Attitude

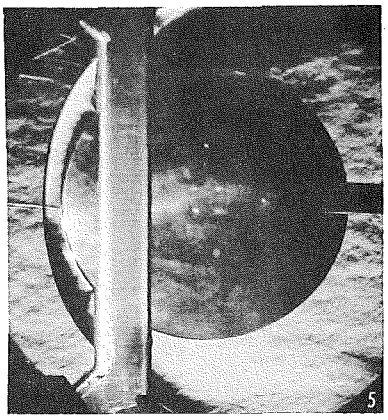

$M_\infty = 3$, $\phi = 0°$

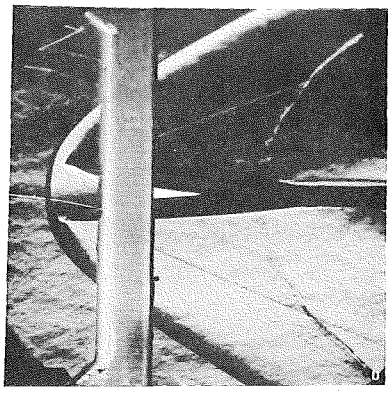

$M_\infty = 3$, $\phi = 90°$

Aft Launch Attitude

Fig. 8 Typical Schlieren Photographs of Force Model

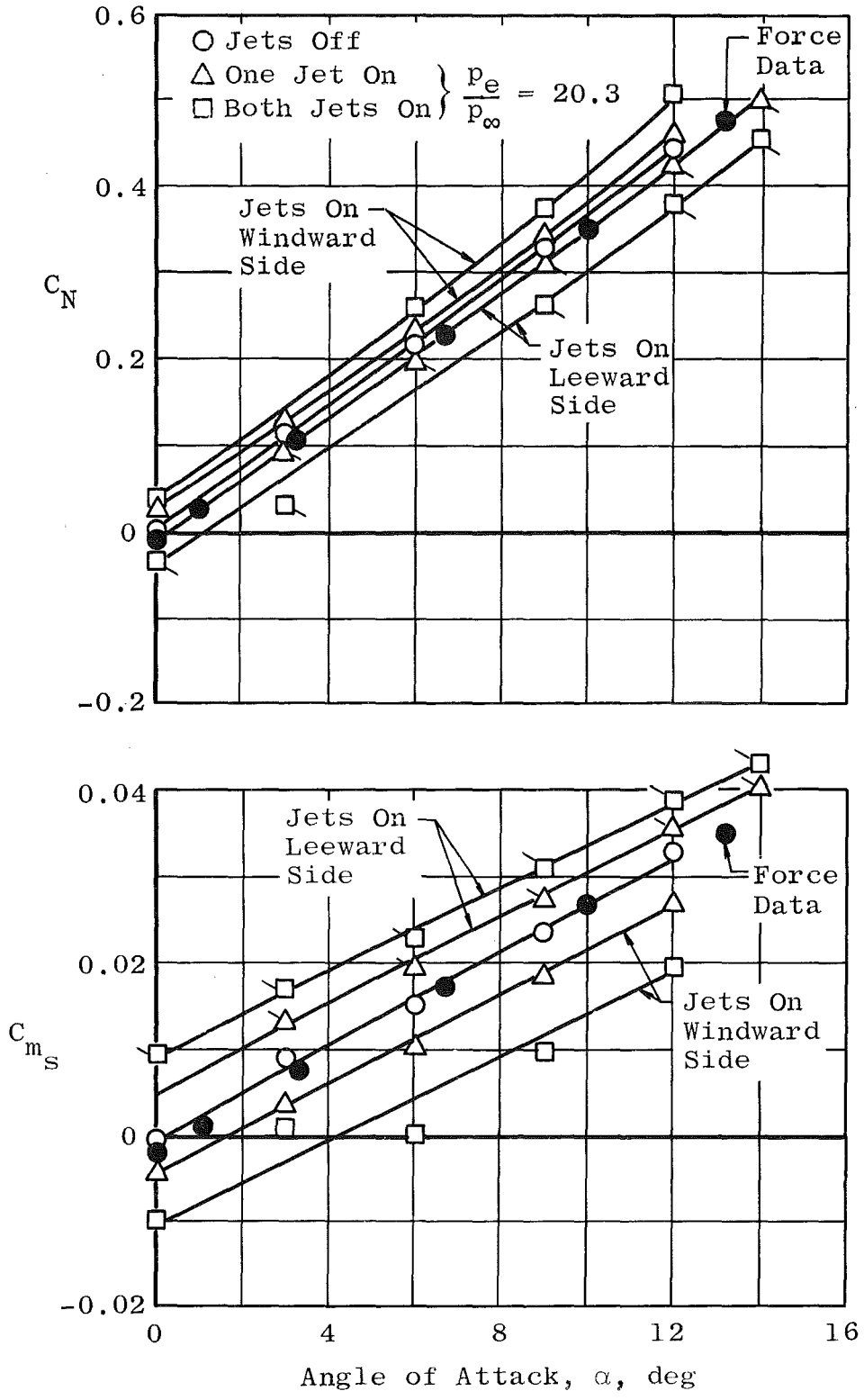

Fig. 9 Longitudinal Stability Characteristics with Jet Flow Effects at $M_\infty = 2$

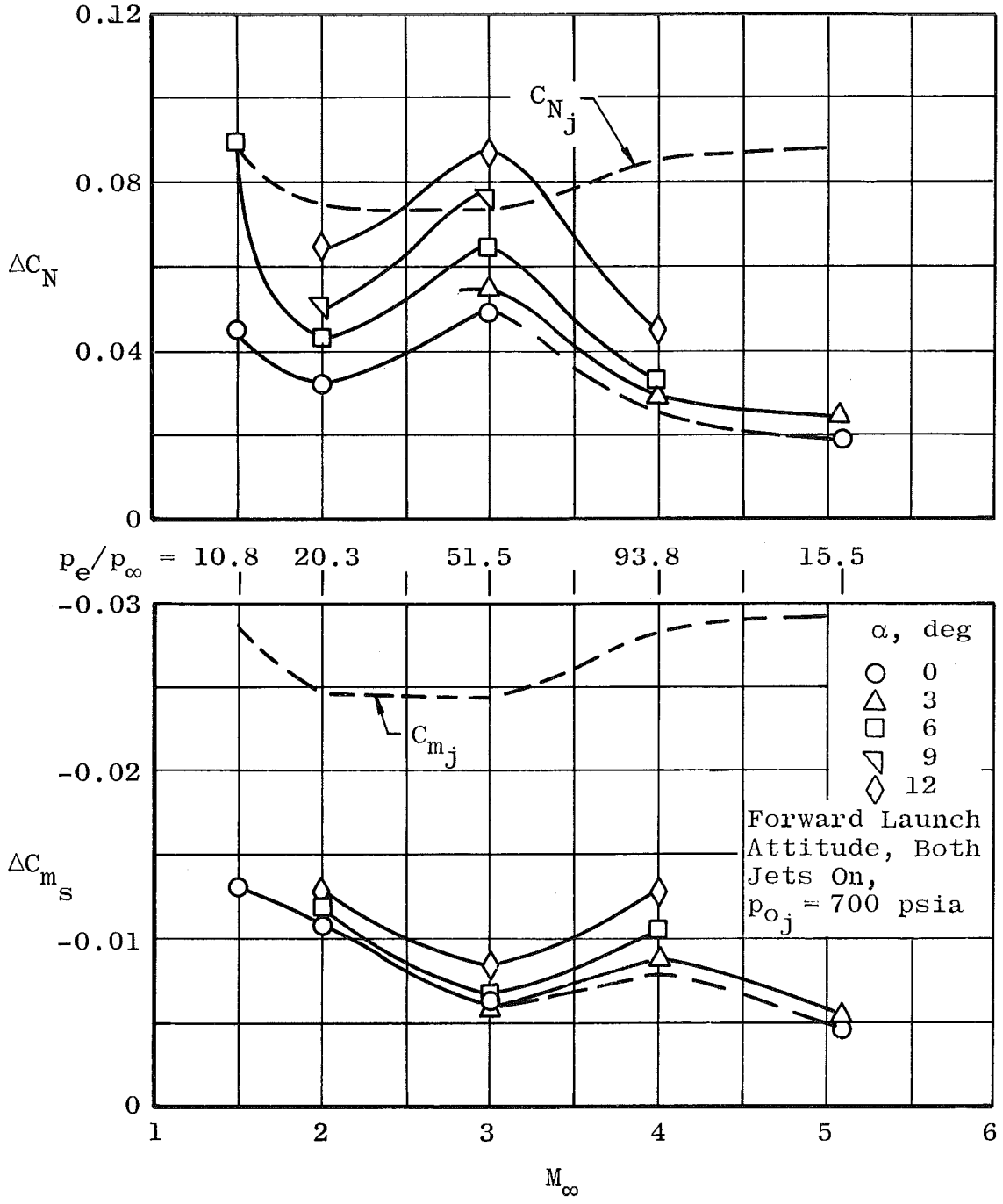

Fig. 10 Effect of Windward Surface Jet Flow on Pitching-Moment and Normal-Force Coefficients

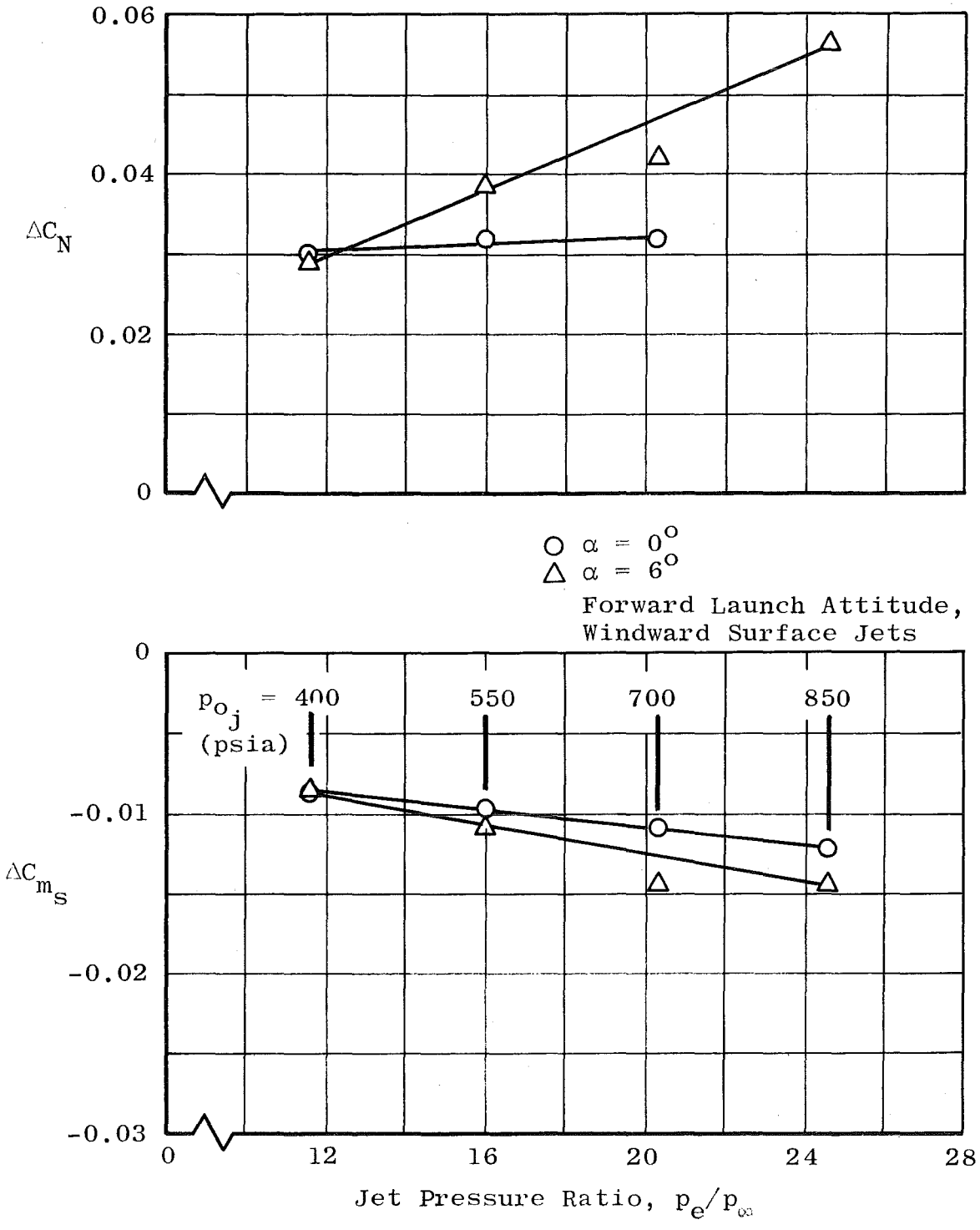

Fig. 11 Effect of Jet Pressure Ratio on Normal-Force and Pitching-Moment Coefficients at $M_\infty = 2$

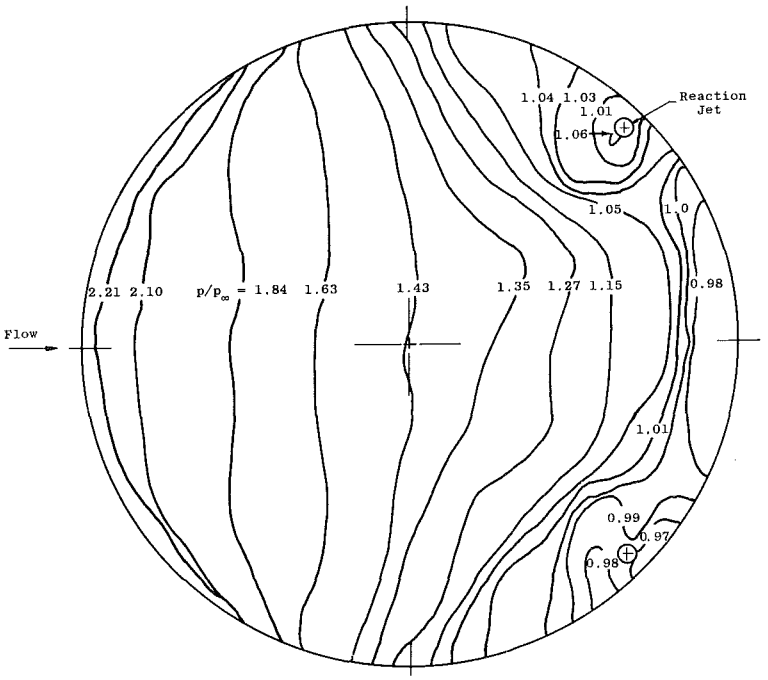

Jets Off

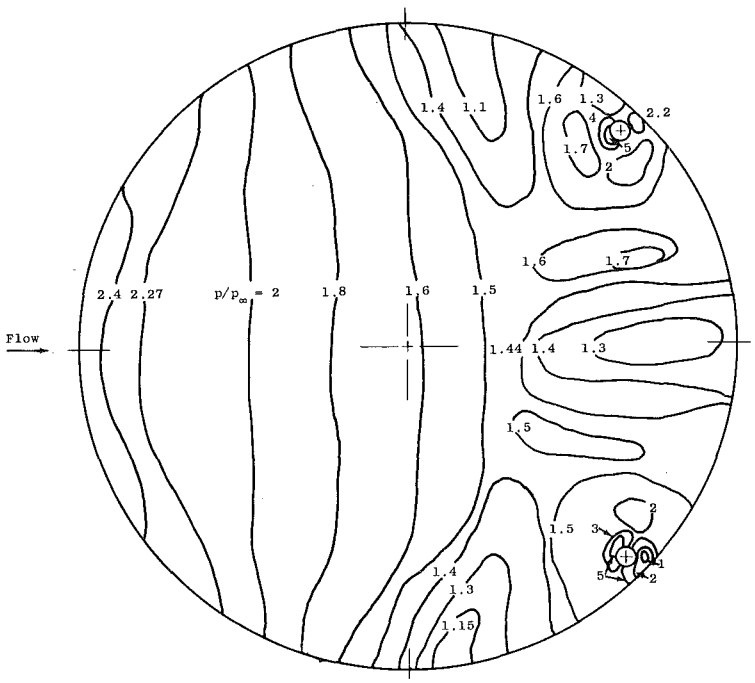

Jets on, p_e/p_∞ = 20.3

Forward Launch Position

Fig. 12 Pressure Isolines p_e/p_∞ on the Windard Surface at M_∞ = 2, α = 6 deg

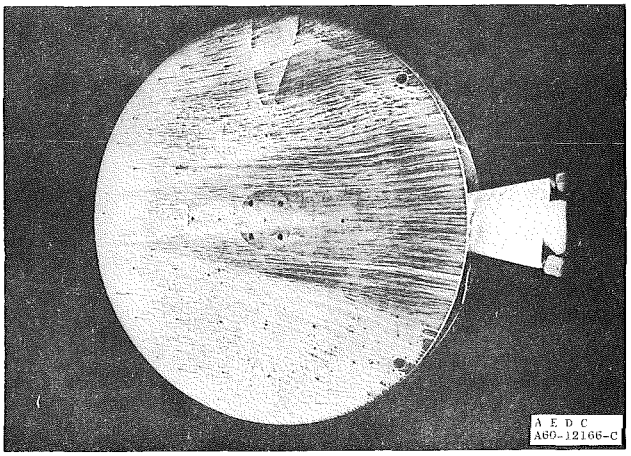

Jets Off

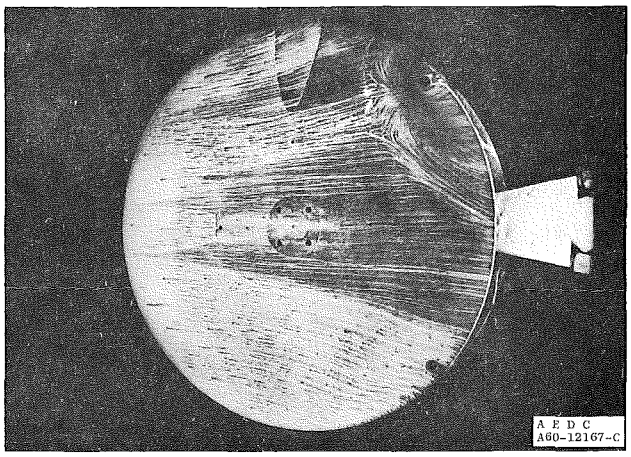

One Jet On, $p_e/p_\infty = 29$

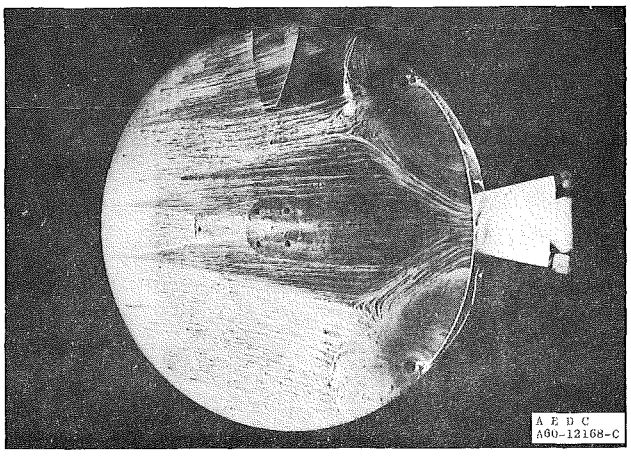

Both Jets On, $p_e/p_\infty = 29$

Fig. 13 Photographs of Flow Patterns on Wind Surface at $M_\infty = 2$, $\alpha = 6$ deg

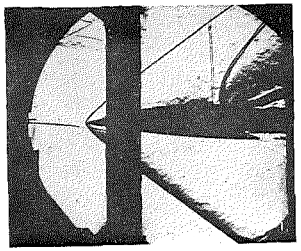

p_{o_i} = 400 psia

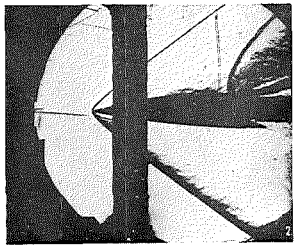

p_{o_i} = 550 psia

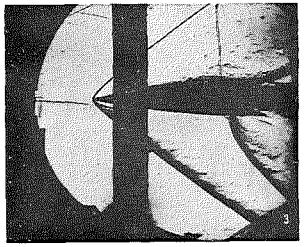

p_{o_i} = 700 psia

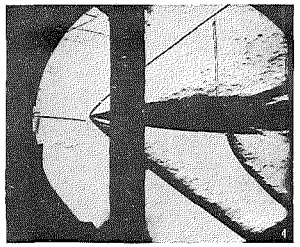

p_{o_i} = 850 psia

Forward Launch Attitude with Both Jets On, $M_\infty = 2$, $\alpha = 0$, $\phi = 90°$

M_∞ = 1.5

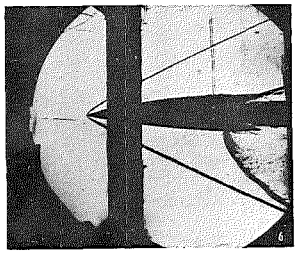

M_∞ = 3

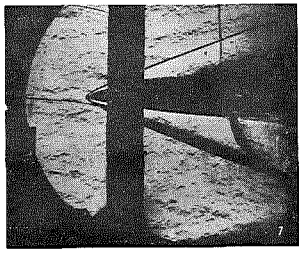

M_∞ = 4

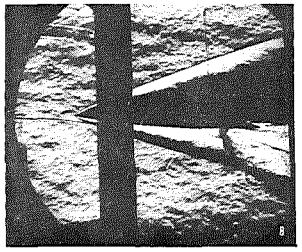

M_∞ = 5

Forward Launch Attitude, Both Jets On, p_{o_i} = 700 psia, $\alpha = 0°$, $\phi = 90°$

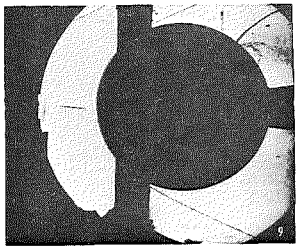

One Jet On

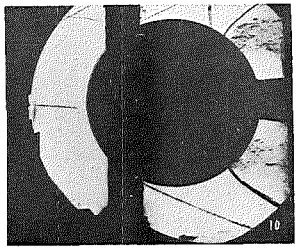

Both Jets On

Forward Launch Attitude, $M_\infty = 3$, p_{o_i} = 700 psia, $\phi = 0°$

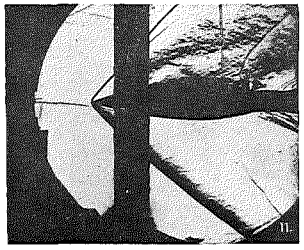

Side-Launch Attitude, $M_\infty = 2$, Both Jets On, p_{o_i} = 700 psia, $\psi = 14°$, $\phi = 90°$

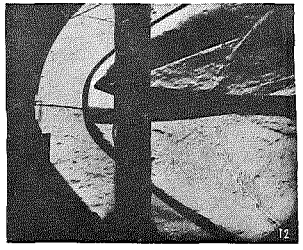

Aft-Launch Attitude, $M_\infty = 3$, $\phi = 90°$, Both Jets On, p_{o_i} = 700 psia

Fig. 14 Typical Schlieren Photographs of Pressure Model